Quadruply Discrete Classification for Low-Dimensional Chaos

Robert Gilmore

Physics Department, Drexel University, Philadelphia, PA, USA 19104
robert.gilmore@drexel.edu

Résumé It is finally possible to classify low-dimensional strange attractors — strange attractors with Lyapunov dimension $d_L < 3$. There are four levels of structure in this classification : (1) basis sets of orbits ; (2) branched manifolds ; (3) bounding tori ; and (4) embeddings into R^3. All four levels involve links of knots in very powerful ways. We describe these four levels of structure. There is an incomplete understanding in several levels of this complete organizational hierarchy. We describe how singularities form the backbone of stretching and squeezing processes that generate chaotic behavior. We ask : What is invariant about topological analyses ? We conclude with a brief description of all the covers of a universal image dynamical system — in this case the horseshoe.

1 Introduction

We all sit as students at the feet of Poincaré. He was the first to see, to fret over, to describe, to provide insights into, and to develop tools for studying what we now call chaos. He developed the field of mathematics which contains all of the tools that we find useful for describing dynamical systems, which we now call topology. He also told us that the principle tools, by means of which we might understand the global topological structure of what are now called strange attractors, are the unstable periodic orbits contained in these objects [1].

Thanks primarily to the judicious use of these tools, and in no small part to a number of 'lucky accidents' intrinsic to three-dimensional spaces, we have progressed very far towards a complete understanding of chaos in three dimensions. We are able to describe and classify the strange attractors generated by dissipative dynamical systems in R^3. The classification has four levels of structure and each level is discrete. These four levels are : (1) basis sets of orbits ; (2) branched manifolds ; (3) bounding tori ; and (4) embeddings of these tori in R^3. It is hoped that a final form for the theory of strange attractors in R^3 can serve as a model for the formulation of general theories for : (a) strange attractors of dissipative dynamical systems in higher dimensions ; and (b) chaotic behavior of conservative dynamical systems in any dimension.

In Sec. 2 we show two of the classical strange attractors introduced by Lorenz and Rössler. We also mention two of historical interest — generated by driven nonlinear oscillators. It is remarkable that these four are inequivalent, and that this inequivalence is simple to demonstrate. In Sec. 3 we argue that there is a very close relation between mechanisms that generate strange attractors in toroidal flows $R^d \times S^1$ in any dimension and singularities of mappings $R^m \to R^n$. The two simplest cases, the fold $A_2 : \ R^1 \to R^1$ and the cusp $A_3 : \ R^2 \to R^1$ have much to do with the stretching and squeezing mechanisms that generate chaos in three-dimensional flows in $R^2 \times S^1$ with one unstable and one stable Lyapunov exponent, and in four-dimensional flows in $R^3 \times S^1$ with two unstable and one stable Lyapunov exponent. We make this digression from our major theme for two reasons : (1) to make the point that much of what we know about strange attractors comes from studying these objects in toroidal flows (e.g., the Rössler attractor) ; and (2) to emphasize that there is now a mechanism to "lift" (cf. Sec. 6) flows from a torus $R^d \times S^1$ into more complicated geometries, as described in Sec. 4 in the three dimensional case.

In Sec. 4 we describe the four layers of organizational structure that have been found useful to describe low dimensional ($d_L < 3$) chaos. These all depend on knots in R^3 in some way. At the bottom of this hierarchy is a simple set of periodic orbits that serves to force all the other periodic orbits contained in a strange attractor. This set is called a basis set of orbits. A sequence of changes in the basis set

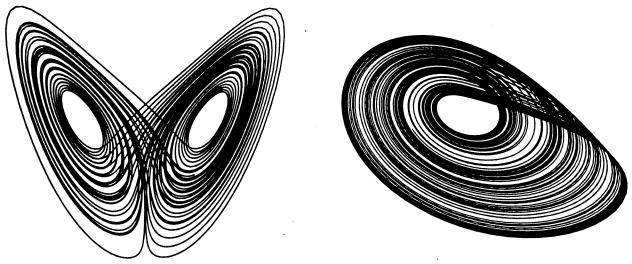

Fig.1. Lorenz attractor (left) and Rossler attractor (right). Both are generated at standard control parameter values.

serves, like trail markers, to describe the transition from nonchaotic ("laminar") to fully chaotic behavior. Transitions to chaos are properly described by citing a sequence of basis sets of orbits. At the next level are the branched manifolds that serve to hold, and to organize, all the unstable periodic orbits that exist in a strange attractor. The organization is determined by the orbits' topological invariants. Branched manifolds have been used to identify processes that generate chaos in a number of experimental systems. At the third level of structure are the bounding tori that serve to organize branched manifolds in the same way that branched manifolds serve to organize periodic orbits. Bounding tori are classified intrinsically — that is, by how they look from the inside. At the fourth and last level of structure is the extrinsic classification of bounding tori — how they look from the outside. This means simply : how these tori are embedded in R^3. Links of knots play an important role in all four layers of structure.

In Sec. 5 we pose an important question : What is the relation between an attractor "reconstructed" by using any of the standard embedding theorems, and the original attractor that generated (usually scalar) time series ? In short, exactly how much of the information that is determined from a topological analysis is fundamental, and how much is embedding-dependent ?

In Sec. 6 we emphasize the close relation between questions that can be asked of the theory of Lie groups, the theory of singularities, and of dynamical systems theory. Since phrasing a question is 90% of the progress towards an answer, it is useful to review the more mature fields for fruitful questions and pose corresponding questions of our younger field. One question (Cartan's question) from Lie group theory is : How many images does a covering group have ? The corresponding question of dynamical systems theory is : If the Smale horseshoe (e.g., Rössler attractor) is a universal image, how many covers does it have ? It is finally possible to answer this question in a constructive way. Results are summarized in the final section.

2 The Classical Strange Attractors

It is generally agreed that the first strange attractor discussed extensively in the literature was the Lorenz attractor [2], shown in Fig. 1. The Lorenz equations are a severe truncation of the Navier-Stokes equations. For standard control paarameter values they exhibit three fixed points : a saddle at the origin and two unstable foci off the z-axis. These foci lie in the "eyes" of the Lorenz mask.

Rumor has it that Rössler considered this attractor much too complicated, and set out to design a strange attractor with only one unstable focus [3]. The Rössler attractor is also shown in Fig. 1. Not only did he succeed in creating a simpler attractor : He simultaneously created a very simple model dynamical system that qualitatively describes the flows for many of the low dimensional strange attractors that have been successfully analyzed to date. As opposed to the Lorenz mask, the Rössler mask is suitable for Polyphemus.

These two attractors have provided an enormous amount of intuition for our understanding of the properties of chaotic flows in three dimensions, and the strange attractors that these flows generate.

Besides these two widely known attactors, there are a number of other low dimensional strange attractors that are somewhat less well-known. Two important attractors from this class include the Duffing attractor and the van der Pol-Shaw attractor. A caricature of all four of these attractors will be presented later. It is a remarkable fact that none of these attractors is related to any of the others by a smooth change of coordinates. More formally, it is easy to show that no diffeomorphism exists that maps any of these attractors to any of the others.

3 A First Step in Understanding

We have learned an enormous amount about strange attractors by adopting the geometry exhibited by Rössler's attractor. It can be seen reasonably easily that this attractor fits inside a simple torus. The phase space for this attractor is $R^2 \times S^1$, or more accurately $D^2 \times S^1$, where D^2 is a bounded two-dimensional disk in R^2. This same phase space describes any periodically driven two dimensional nonlinear oscillator, of which particular examples are the Duffing and the van der Pol oscillators.

One way to study the Rössler attractor is to take a plane of constant phase — a Poincaré section, and allow it to flow around a "full circle." In a sense, we replace the flow by a map of the plane into itself. In a particular limit, one of high dissipation, the attractor usually shrinks to a very thin structure, almost two-dimensional ($d_L = 2+\epsilon$). Its intersection with a Poincaré section is therefore almost one-dimensional. In this limit the Poincaré map almost reduces to a map of the interval onto itself. This limit is shown in Fig. 2 [4] (cf. [5], Fig. 11.4).

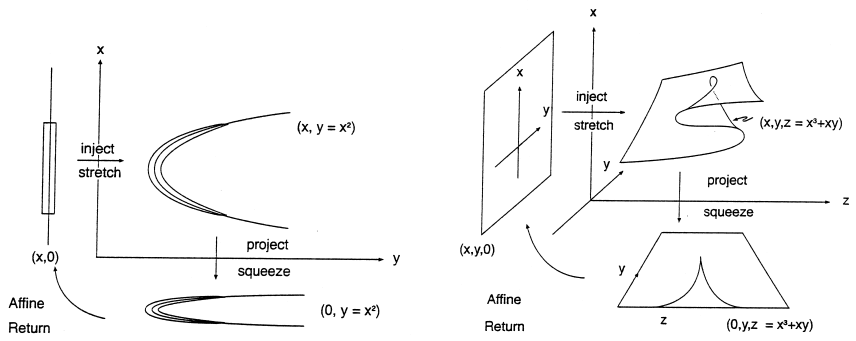

Fig.2. (left) Intersection of a strange attractor in $R^2 \times S^1$ with a Poincaré section is almost an interval. The Poincaré return map exhibits a fold singularity, producing a logistic map. (right) Intersection of a strange attractor with two positive Lyapunov exponents in $R^3 \times S^1$ with a Poincaré section is almost a plane section. The Poincaré return map exhibits a cusp singularity. Cf. [5], Fig. 11.4, Fig. 11.5.

It is well-known from the theory of singularities that mappings of the interval to itself can exhibit singularities. In this case the only singularities that can exist are isolated fold singularities. The simplest fold singularity occurs in the map of the interval to itself given by the well-known logistic map : $x' = a - x^2$. It is in this sense that the fold singularity (A_2 in the singularity theory literature) forms the backbone of the simple stretch-and-fold mechanism that is responsible for the formation of the Smale horseshoe, and which the Rössler equations exhibit. As control parameters change, two or more isolated folds can occur in the transition from folding chaos to funnel chaos to gateau roulé chaos. It should not be surprising that many of the features that occur in the canonical route to chaos in the logistic map are also seen in the Rössler equations : period doubling, accumulation, noisy period halving, periodic windows descending and widening to period three, then ascending and narrowing again ... . When two or more isolated folds occur in the mapping of $R^1 \to R^1$ we see features beyond those contained in the logistic map.

We are nearing a complete understanding of chaos in three dimensions. Beyond three dimensions, there is the open question : "How to describe chaos in four and higher dimensions ?" One approach to this question involves studying analogs of the Rössler flow : in $R^3 \times S^1$. In this case there are three nonzero Lyapunov exponents, rather than two in the lower dimensional case. New insight will occur when we understand how to describe flows with $\lambda_1 \geq \lambda_2 \geq \lambda_3 = 0 > \lambda_4$, with $\lambda_1 + \lambda_2 + \lambda_3 + \lambda_4 < 0$. In this case, for very dissipative systems with Lyapunov dimension $d_L = 3 + \epsilon$, a strange attractor will be "very thin" and its intersection with a Poincaré section will be almost two-dimensional. The Poincaré map now becomes almost a map of $R^2 \to R^2$. Such maps also exhibit singularities. One obvious singularity is the double fold ("folded towel"), but this is structurally unstable and perturbs to a cusp singularity (A_3) [5] (cf., Fig. 11.11), [6]. Such a map is also illustrated in Fig. 2 ([5], Fig. 11.5). The cusp occurs as a backbone for flows in $R^3 \times S^1$ in the same way that the fold occurs as a backbone for flows in $R^2 \times S^1$.

If the logistic map serves to provide intuition for what is to be expected in dissipative three-dimensional systems, the cusp map should also serve to provide intuition for what is to be expected in dissipative four-dimensional systems. The cusp map has been studied over a restricted range of its intrinsic control parameters. What we find is a much richer spectrum of behavior than seen in the logistic map. In fact, this study was undertaken because of prodding by an experimentalist : "Tell me what I can expect to see if my experimental system is four dimensional with two positive Lyapunov exponents." We find the control space is partitioned into overlapping "triangular regions", each describing periodic orbits ([5], Fig. 11.6 and [7]). They are parameterized by rational fractions p/q, where p and q have the usual interpretation compatible with a mode-locking scenario. The boundaries of the triangles are combinations of saddle-node, period-doubling, and Hopf bifurcation curves. Any path through the control parameter space will encounter these regions. They are the analogs of the windows that appear in the logistic map. Some of the resonances attached to the Hopf bifurcation from the primary period-one window are shown in Fig. 3.

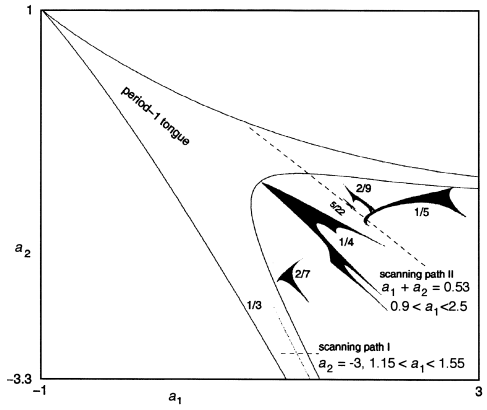

Fig.3. Analog of the logistic map bifurcation diagram, for the cusp map. Triangular regions attached to the primary Hopf bifurcation curve describe stable p/q resonant tori. Cf. [5] Fig. 11.6.

4 Layers of Organizational Structure

How do we understand strange attractors ? How do we classify strange attractors ? These are difficult questions. Understanding and classification must be coordinate system independent — that is, neither must be affected by a deformation of phase space through any nonsingular transformation.

The best way to attempt to understand these objects is to throw ourselves on the mercy, or at least the insight, of Poincaré. He invented topology as the ideal tool for study of chaotic systems. He also urged

us, in no uncertain terms, to study the unstable periodic orbits in these systems as the only keyhole through which we could squeeze our understanding. In fact, following the strategy laid down by Poincaré has brought us to our current level of understanding of low dimensional strange attractors, and especially their global topological structure.

4.1 Branched Manifolds

The first modern contribution to this program was provided by Birman and Williams [8]. They did two things. First, they introduced a simple structure that contained all the unstable periodic orbits that existed in a certain class of strange attractors. These structures are called variously : orbit organizers, orbit holders, templates, branched manifolds, gabarits, ... The orbits on these structures are organized in exactly the same way as the "corresponding" orbits (correspondence by symbol set) in the strange attractor. Organization is determined by their spectrum of linking numbers and relative rotation rates [9] : two topological invariants that are associated with braids. Second, they introduced a very important equivalence concept : two points in a strange attractor are equivalent if they have the same asymptotic future

$$x \sim y \qquad \text{if} \qquad \lim |x(t) - y(t)| \stackrel{t \to \infty}{\longrightarrow} 0$$

The Birman-Williams theorem guarantees that the unstable periodic orbits in a three-dimensional dissipative dynamical system can be projected ("isotoped") down to a branched manifold without altering their topological organization. As a result, branched manifolds can be used to classify strange attractors [10], [11].

This has been used backwards. If a few unstable periodic orbits can be extracted from experimental data and their topological organization (in some embedding) can be determined, it is possible to identify the branched manifold that supports them and all the other unstable periodic orbits that exist in the strange attractor [12]. In particular, it is possible to predict the linking numbers of orbit pairs in the strange attractor. If these predictions do not conform to the observations, the original template assignment and orbit identification must be rejected. Topological analysis (of experimental data) is the only analysis procedure for chaotic data with built-in rejection criteria [4], [5].

Four branched manifolds are shown in Fig. 4. These describe the organization of the unstable periodic orbits in : the Rössler attractor (Fig. 4(a)) ; the Duffing attractor (Fig. 4(b)) ; the van der Pol attractor (Fig. 4(c)) ; and the Lorenz attractor (Fig. 4(d)). These four branched manifolds are inequivalent. As a result, it is not possible to find any coordinate transformation that maps any into any of the others. The four sets of equations are inequivalent — by topological arguments.

4.2 Basis Sets of Orbits

Branched manifolds always allow more unstable periodic orbits than are seen in either experimental data or simulations. In moving from the hyperbolic limit, described by branched manifolds, to the more realistic but nonhyperbolic limit seen in Nature, many of the unstable periodic orbits are pruned away, but those that remain are organized exactly as in the hyperbolic limit [13].

A useful procedure has been developed to identify the spectrum of unstable periodic orbits in a strange attractor whose branched manifold is known. This involves specifying a basis set of unstable periodic orbits. The basic idea is as follows. The existence of some periodic orbits *forces* the presence of other periodic orbits [14]. The number of orbits forced by a specific orbit is estimated by the entropy of that orbit. Starting with a spectrum of orbits up to some period p, we remove the highest entropy orbit. We also remove all the orbits in this set that are forced by this highest entropy orbit. This leaves a residual set with a smaller number of periodic orbits. The process is repeated until no orbits remain [4], [5]. The ordered set of highest entropy orbits removed from the original set and all the resulting residual sets forms the basis set of orbits.

A forcing diagram for the horseshoe is shown in Fig. 5. Forcing is transitive, so if orbit A forces orbit B ($A \Rightarrow B$) and $B \Rightarrow C$, then $A \Rightarrow C$. For example, $6_4 \Rightarrow 8_6 \Rightarrow 7_2$. Transitivity allows us to construct

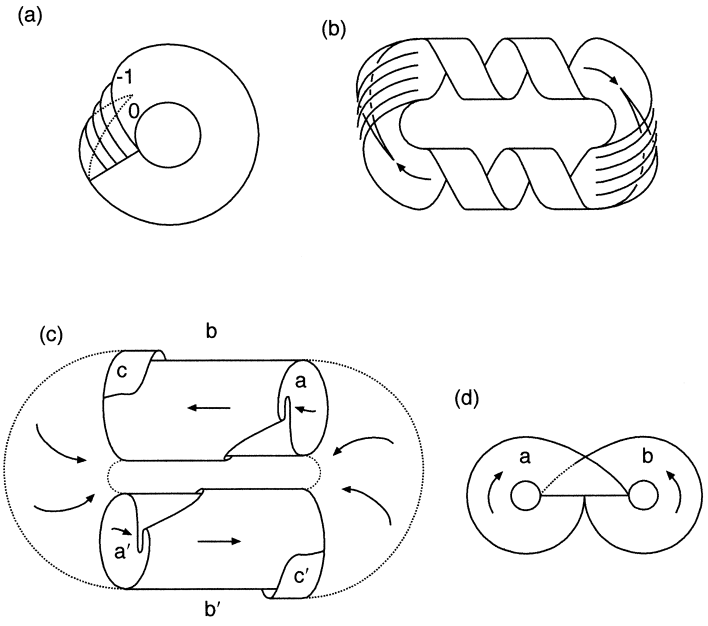

Fig.4. Branched manifolds for four standard strange attractors. (a) Rössler attractor ; (b) Duffing attractor ; (c) van der Pol attractor ; (d) Lorenz attractor. Cf. [5], Fig. 4.1

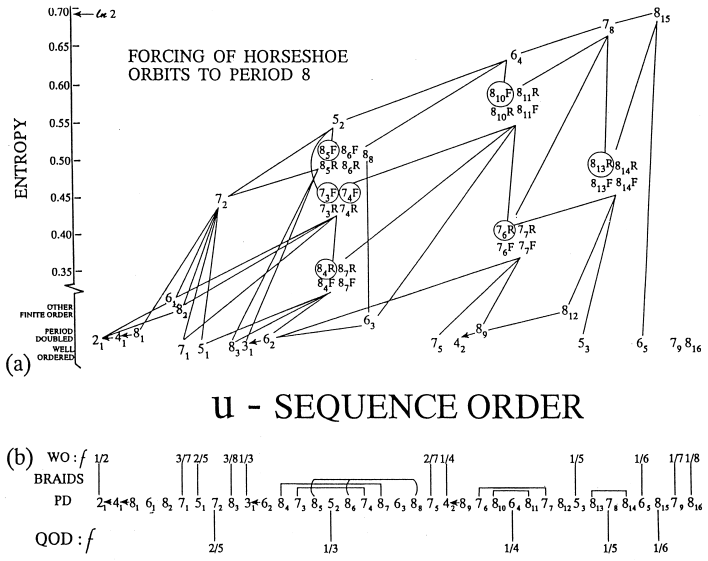

Fig.5. Forcing diagram for orbits in the horseshoe flow. The orbits are labeled by their order of occurrence in the logistic map. Cf. [4], Fig. 38.

simple forcing diagrams. As control parameters vary and the shape of an incomplete horseshoe changes, new orbits are created and/or old orbits are annihilated. The transition from laminar (no chaos, lower left in Fig. 5) to fully hyperbolic (topological entropy = ln(2), upper fight in Fig. 5) follows some path in this figure. Any path is a route to (horseshoe) chaos. There are many possible paths. The phrase "period doubling route to chaos..." really tells us very little about the details of the road from the lower left (laminar) to upper right (hyperbolic chaos) in this figure. There are literally millions of routes to chaos for horseshoe dynamics. Each path to chaos is represented by a sequence of basis sets of orbits, just as a hiking trail is labeled by a series of trail markers.

A forcing diagram exists (in principle) for every branched manifold. Regrettably, the forcing diagram for the horseshoe is incompletely known despite a great deal of effort [15],[16]. Forcing diagrams for other branched manifolds are largely terra incognita.

4.3 Bounding Tori

As control parameters vary the branched manifold that describes a chaotic dynamical system can also vary. That is, new branches can be created and/or old branches can be destroyed. One fingerprint for this activity is a change in the spectrum of symbols required to create a symbolic dynamics for the flow. This is seen, for example, both for the Lorenz and the Rössler attractors as various control parameters are changed.

As control parameters change, we can see : (a) changes in the basis set of orbits on a branched manifold and (b) changes in the number and type of branches in the branched manifold that the flow projects to. We know that branched manifolds serve as periodic orbit organizers. We ask for an analogy : Is there some structure that acts as branched manifold organizers ?

The answer is : Yes. Bounding tori are branched manifold organizers in exactly the same way that branched manifolds are periodic orbit organizers [17], [18]. We sketch the outlines of the arguments.

The flow in a strange attractor is projected down to a branched manifold using the Birman-Williams identification. The projected flow (a *semiflow*, [8]) on the branched manifold has no fixed points. Every point in the branched manifold is surrounded by a small ball of radius ϵ. The radii are taken sufficiently small to exclude all fixed points of the flow that generates the strange attractor. The union of these spheres forms a three dimensional manifold in the phase space. There are no fixed points in this manifold, which is a submanifold of the inertial manifold [19]. The boundary of this three-dimensional manifold is a closed, compact, connected, oriented two-dimensional manifold without boundary. All surfaces with this property are known and have been classified : they are tori of genus-g [20]. They are boundaries of "handlebodies" with g handles.

These surfaces separate the flow, which is inside, from the singularities of the vector field in R^3 that generates the flow, which are on the outside. The flow in the neighborhood of the branched manifold can be restricted to the bounding torus. The flow restricted to the surface does have singularities. These occur where the flow is perpendicular to the surface. The flow that generates the strange attractor has three Lyapunov exponents : one (λ_1) is positive, the one in the direction of the flow (λ_2) is zero, and the third (λ_3) is negative. Where this flow is perpendicular to the surface, there is a fixed point on the surface. The eigenvalues at the fixed point are the nonzero exponents λ_1 and λ_3. As a result, each fixed point of the flow restricted to the surface is a regular saddle.

A fixed point has index $(-1)^{n_u}$, where n_u is the number of unstable directions. Every singularity on the bounding surface is a regular saddle, with $n_u = 1$ and therefore $(-1)^{n_u} = -1$. There is a beautiful and powerful topological invariant that can be associated with any manifold $\mathcal{S}$ [5], [20]. It is called the Euler characteristic $\chi(\mathcal{S})$. It can be computed for any surface. What is remarkable is that if you construct any vector field on $\mathcal{S}$, the sum of the indices at all the singularities is exactly equal to this topological index. This is the content of the Poincaré-Hopf index theorem [21]. The Euler index for a bounding torus of genus-g is

$$\chi(\text{genus} - g) = 2 - 2g$$

As a result, the flow, restricted to the boundary, has exactly $2g - 2$ singularities.

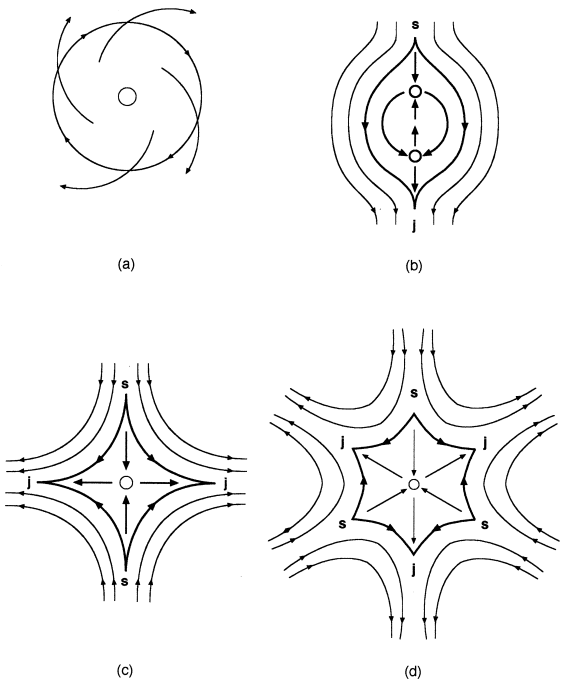

Fig.6. Interior holes (darker) of bounding tori separate the flow (outside, with arrows)from the singularities in the vector field (inside, open circles) that produce the flow. These singularities force the presence of (a) 0, (b) 2, (c) 4, (d) 6, ... singularities on the interior boundaries. The number of singularities identifies the type of singular point in the vector field and has a profound impact on the structure of the flow in the neighborhood of the singularity, except in the case of two singularities (b). Cf. [18].

It is possible to express the flow, restricted to these bounding tori, in a canonical form [17], [18]. In this canonical form the bounding surface is projected onto a planar surface. In this projection there is an outer boundary and g interior holes. All the singularities occur on these boundaries. In fact, in the canonical form there are no singularities on the outer boundary and on m of the g interior holes. Further, the flow on the outer boundary and the m interior holes without singularities is in the same direction. On the $g - m$ interior holes with singularities, the singularities occur in pairs. Singularities are of two types : s and j. The s-type singularity splits the flow, and the j-type singularity occurs where flows from different parts ("flow tubes") join. Holes with 0, 2, 4, and 6 singularities are shown in Fig. 6. It is evident that holes with exactly two singularities, an (s, j) pair, have no effect on the global structure of the flow, while holes with 0, 4, 6, $\cdots$ do. The holes with two singularities can be "zipped up" [20], leaving only m holes with no singularities and $g - m$ interior holes with four or more (even number of) singularities ([17], [18] and [22], Chapter 15).

Branch lines occur following (in the sense of the flow) each j-type singularity and before its downstream s-type singularity. All branch lines between a (j, s) pair can be moved to a single branch line. Since there are $g - 1$ singularity pairs of type (j, s), any branched manifold in a genus-g bounding torus has exactly $g - 1$ branch lines ($g > 1$).

The homotopy group of the genus-g torus has $2g$ generators. Of these, half are meridians and half are longitudes [23]. One longitude can be taken around each of the g interior circles. The g meridians can be chosen in such a way they they are boundaries of disks lying completely inside the bounding torus, and these disks are transverse to the flow. In short, these disks satisfy Poincaré's conditions for (components of) a Poincaré section. Of these, $g-1$ are independent [17]. All the independent components occur between (j, s) pairs, of which there are $g - 1$. The remaining disk is not independent, and need not

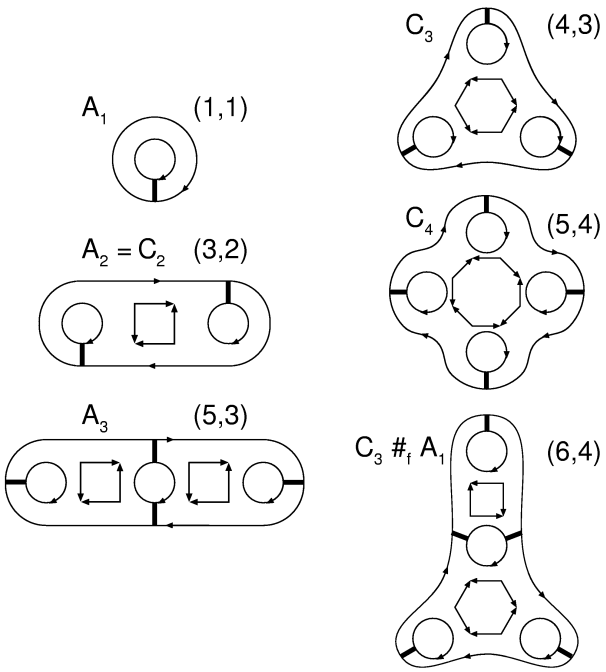

Fig.7. Canonical projections of bounding tori of genus g. The flow around the exterior boundary and the m interior holes without singularities is in the same direction. The remaining $g-m$ interior holes have 4, 6, 8, $\cdots$ singularities. Canonical tori are partly identified by the two integers (g,m). The $g-1$ dark lines connecting the m interior holes without singularities to the exterior boundary simultaneously represent the components of the global Poincaré section and branch lines of any branched manifold compatible with the bounding torus. Two infinite series A_n and C_n are linear and cyclic, respectively. Many other types of bounding tori exist. All can be uniquely labeled by "an orbit of period $g-1$."

be included among the components of the Poincaré section. Each of the $g-1$ branches of a branched manifold can be moved to the component of the Poincaré section sharing the same (j,s) pair with it. In projection, all $g-1$ components (disks) of the global Poincaré surface of section connect one of the m interior circles without singularities to the exterior boundary. A number of canonically dressed tori are shown in Fig. 7. In fact, what is shown is actually a planar projection of these surfaces. The interior holes without singularities are shown as circles. The $g-m$ holes with singularities are shown as polygons with $2\lambda_*$ sides. Arrows along the edges indicate the singularity structure. Dark lines connecting interior holes with the exterior boundary represent simultaneously the $g-1$ components (disks) of the global Poincaré section as well as branch lines of any enclosed branched manifold.

Canonically dressed tori can be classified. At the grossest level, the pair of integers (g,m) is useful. However, degeneracies occur for $g=7$. These degeneracies can be lifted by introducing a third label. This label is a Young partition. The idea is the following. Each of the interior holes with singularities has an even number of singularities : 4, 6, 8, ... They occur as pairs. List the number of pairs for each of the interior holes with singularities : $\lambda_1 \geq \lambda_2 \geq \cdots \geq \lambda_{g-m} \geq 2$. These integers satisfy the same inequalities as row lengths for Young partitions with row length ≥ 2. Even this fails to remove degeneracies for $g \geq 7$, so additional labels are required. We show these labels in Fig. 8.

Since each of the branch lines is attached to the outer boundary, they can be numbered in order from any starting point just by following the flow direction along the outer boundary. This is done for the 6 branch lines in each of the five canonical bounding tori of genus 7. The round holes are also numbered in the order in which they are encountered. Finally, the holes with singularities are labeled with letters : $a,\ b, \cdots$. Canonically dressed tori are uniquely labeled in three ways, following the flow direction along the outer boundary :

Singular holes : Identify, by letter, the order in which the singular holes are encountered.

Round holes : Identify, by number, the order in which the nonsingular holes are encountered.

Branch lines : Identify the number of branch lines attached to each nonsingular hole as that hole is encountered.

These three schemes have been used to uniquely identify each of the five canonically dressed tori of genus seven in Fig. 8.

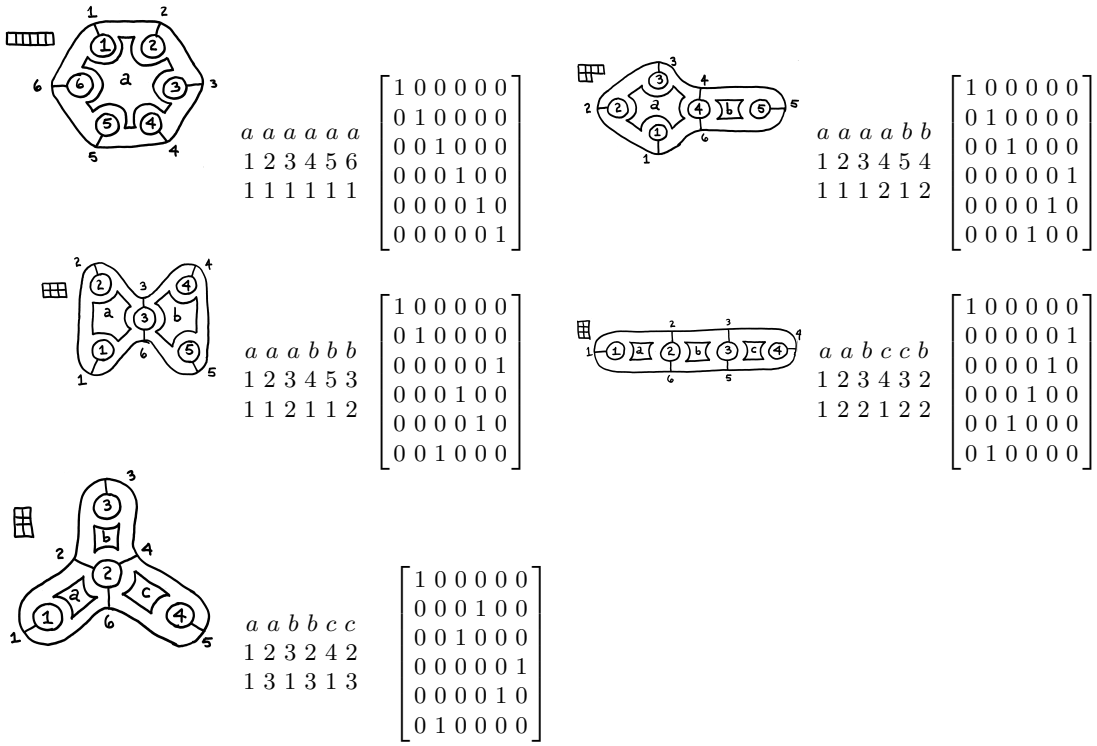

Fig.8. There are five canonically dressed tori of genus 7. Two inequivalent flows have Young partitions 2^3.

In this canonical representation, the flow from any branch line, or equivalently, from any component of the global Poincaré section, visits two other branch lines/components of the global Poincaré section. This property is summarized, as usual, by a transition matrix T, with $T_{i,j} = 1$ if the flow from i to j is allowed. The transition matrix T has the property that two entries in every row and every column are $+1$, the remainder being zero [17] [18], [22]. In the canonical numbering of branch lines following the flow around the outer boundary, the matrix elements $T_{i,i+1}$ (mod $g-1$) are nonzero. We call this a cyclic matrix, and write it as $T_{\rm cyc}$. The transition matrix can therefore be written as

$$T = T_{\rm cyc} + T_{\rm str}$$

The second matrix on the right, $T_{\rm str}$, determines the topological structure of the bounding torus. Both matrices $T_{\rm cyc}$ and $T_{\rm str}$ have exactly one nonzero entry $+1$ in each row and column. Since the $(g-1)\times(g-1)$ cyclic matrices are the same for all canonical tori with the same genus g, these tori can be distinguished entirely by specifying only one part of the transition matrix, $T_{\rm str}$. These matrices are presented in Fig. 8 for the five canonical tori of genus seven shown in that figure.

The number, $N(g)$, of canonically dressed tori of genus-g grows rapidly with g :

g	1	2	3	4	5	6	7	8	9
$N(g)$	1	0	1	1	2	2	5	6	15

The fifteen canonically dressed tori of genus 9 are identified in Table 1.

Tab.1. Canonical flows that dress a genus-9 torus are listed in "alphabetic" order. Their Young partitions are given. The permutation group cycle that defines the torus is also given.

	Period − 8 Orbit	Young Partition	Defining P_8 Cycles
1	1 1 1 1 1 1 1 1	(8)	
2	1 1 1 1 1 2 1 2	(6, 2)	(6, 8)
3	1 1 1 1 2 1 1 2	(5, 3)	(5, 8)
4	1 1 1 2 1 1 1 2	(4, 4)	(4, 8)
5	1 1 1 2 2 1 2 2	(4, 2, 2)	(4, 8)(5, 7)
6	1 1 1 3 1 3 1 3	(4, 2, 2)	(4, 6, 8)
7	1 1 2 1 2 1 2 2	(3, 3, 2)	(3, 8)(5, 7)
8	1 1 2 1 2 2 1 2	(4, 2, 2)	(3, 5)(6, 8)
9	1 1 2 2 1 1 2 2	(3, 3, 2)	(4, 7)(3, 8)
10	1 1 2 2 1 2 1 2	(3, 3, 2)	(4, 6)(3, 8)
11	1 1 3 1 1 3 1 3	(3, 3, 2)	(3, 6, 8)
12	1 2 1 2 1 2 1 2	(4, 2, 2)	(2, 8)(4, 6)
13	1 2 2 2 1 2 2 2	(2, 2, 2, 2)	(2, 8)(3, 7)(4, 6)
14	1 2 3 1 3 1 3 2	(2, 2, 2, 2)	(2, 8)(3, 5, 7)
15	1 4 1 4 1 4 1 4	(2, 2, 2, 2)	(2, 4, 6, 8)

Canonically dressed tori are uniquely identified by a sequence of $g-1$ symbols subject to certain conditions. The labeling shown in Table 1 is the most convenient of the three equivalent labeling schemes introduced above, as the matrix $T_{\rm str}$ can be constructed immediately from this sequence of symbols [18],[22]. These symbol sequences can be regarded as "period $g-1$ orbits." Canonically dressed tori are uniquely identified by period $g-1$ "orbits."

There are two simple infinite series of canonically dressed tori worth describing :

A_n **:** There are n round holes separated by $n-1$ holes with four singularities each. The genus is $2n-1$. A_4 is shown in Fig. 8 : It has Young partition 2^3 and is labeled by the period-6 orbit $(122)^2$.

C_n **:** There are n round holes surrounding a single hole with $2n$ singularities. The genus is $n+1$. C_6 is shown in Fig. 8 : It has Young partition 6 and is labeled by the period-6 orbit 1^6.

All known strange attractors studied in R^3 belong to one of these classes of bounding tori. Multispiral attractors [24] are of type A_n. Many of the covers of the Rössler attractor with C_n symmetry (under the group operation $R_z(2\pi/n)$) are of type C_n [25], [26]. In Table 2 we list all low dimensional strange attractors described to date, and indicate the equivalence class of each. The van der Pol strange attractor is contained within a pair of concentric tori, each of type A_1. It has both an inner and an outer boundary. Its boundary is therefore the union of two tori of type A_1 : $A_1 \cup A_1^{(1)}$. The superscript $^{(1)}$ indicates that the interior torus intersects the Poincaré section of the exterior torus once. Group continuations of the van der Pol attractor exist that are bounded by $A_1 \cup A_1^{(2)}$ [22].

4.4 Extrinsic Structures

The classification of bounding tori is *intrinsic* [20]. We have described how the flow looks from *inside* the bounding torus. We have not yet described how the flow sits in R^3, or whatever three-dimensional manifold M^3 contains the strange attractor.

Tab.2. All known strange attractors of dimension $d_L < 3$ are bounded by one of the standard dressed tori.

Strange Attractor	Dressed Torus	Period $g-1$ Orbit
Rossler, Duffing, Burke and Shaw	A_1	1
Various Lasers, Gateau Roule	A_1	1
Neuron with Subthreshold Oscillations	A_1	1
Shaw-van der Pol	$A_1 \cup A_1^{(1)}$	$1 \cup 1$
Lorenz, Shimizu-Morioka, Rikitake	A_2	$(12)^2$
Multispiral attractors	A_n	$(12^{n-1})^2$
$\mathcal{C}_n$ Covers of Rossler	C_n	1^n
$\mathcal{C}_2$ Cover of Lorenz$^{(a)}$	C_4	1^4
$\mathcal{C}_2$ Cover of Lorenz$^{(b)}$	A_3	$(122)^2$
$\mathcal{C}_n$ Cover of Lorenz$^{(a)}$	C_{2n}	1^{2n}
$\mathcal{C}_n$ Cover of Lorenz$^{(b)}$	P_{n+1}	$(1n)^n$
$2 \to 1$ Image of Fig. 8 Branched Manifold	A_3	$(122)^2$
Fig. 8 Branched Manifold	P_5	$(14)^4$

$^{(a)}$ Rotation axis through origin.
$^{(b)}$ Rotation axis through one focus.

The *extrinsic* embedding of the bounding torus in R^3 (or M^3) provides the fourth, and final, level of structure required for the description of low-dimensional chaos. We have not proceeded very far in understanding this level of structure, except in the genus-one case.

We describe briefly what is known, with the expectation that extension of these ideas to higher-genus cases will not be too difficult. We consider a strange attractor in $D^2 \times S^1$. This can be embedded in R^3 in a variety of ways. We first describe the "preferred" embedding [23]. If $X(t), Y(t), t \bmod(2\pi)$ are the intrinsic coordinates in $D^2 \times S^1$ and x, y, z are the coordinates in R^3, a preferred embedding is

$$x(t) = (a + X(t))\cos(t) \qquad y(t) = (a + X(t))\sin(t) \qquad z(t) = Y(t)$$

where $a > \max|X(t)|$. The spectrum of topological invariants in the intrinsic torus in $D^2 \times S^1$ and in the preferred embedding in R^3 given above are the same.

In the preferred embedding, the intrinsic torus in lifted to R^3 around a simple planar circle, and is a genus-1 torus that is unknotted. It is possible to map the intrinsic torus into a knotted torus as follows. A knot in R^3 is chosen — a figure-8 knot, for example. For convenience, a finite Fourier representation of each of the three coordinates is chosen : $X_{\rm knot}(t) = \sum_{j=1}^{p} A_j \cos(jt) + B_j \sin(jt)$, where p is finite (and small), and similarly for the Y and Z coordinates. The Fourier knot is chosen to minimize an energy function $E = \oint\oint f(s,t)/|\mathbf{X}(s) - \mathbf{X}(t)|^2 ds\, dt$, subject to some fixed length constraint. Here $f(s,t)$ is some reasonable function. This minimization serves to "separate" the knot as much as possible. We require that the tangent, normal, and binormal vectors $\mathbf{t}(t),\ \mathbf{n}(t),\ \mathbf{b}(t)$ of the *repere mobile* are well-defined for all t, $0 \le t \le 2\pi$, so that the self-linking number $SL_{\rm knot}$ of the knot is well-defined.

To guarantee that an embedding can be created, some distances must be determined and compared. This includes the radius of the intrinsic torus containing the strange attractor. Define $R_{\rm max} = \max(\sqrt{X^2(t) + Y^2(t)})$ for the flow in the intrinsic torus. There are two length scales associated with the knot. One is related to the radius of curvature, the other to the distances between different parts of the knot. Define these two distances for the knot as : $R_{\rm curve}$, the minimum over the radius of curvature of the knot ; and $D_{\rm min}$, the nonzero minimum of the local minima of $|\mathbf{X}_{\rm knot}(s) - \mathbf{X}_{\rm knot}(t)|$. Finally, scale up the size of the knot by a factor a so that $aR_{\rm curve} > R_{\rm max}$ and $aD_{\rm min} > 2R_{\rm max}$.

With these conditions, we embed the strange attractor in the intrinsic torus $D^2 \times S^1$ (coordinates $X(t),\ Y(t),\ t$) into R^3 (coordinates $\mathbf{x}(t)$) by

$$\mathbf{x}(t) = a\mathbf{X}_{\rm knot}(t) + X(t)\mathbf{n}(t) + Y(t)\mathbf{b}(t)$$

The topological invariants (relative rotation rates [9]) of the embedded attractor $\mathbf{x}(t)$ are identical, up to some additive global torsion, to the topological invariants of the intrinsic attractor. The global torsion is the self-linking number of the *carrier knot*, the knot that carries the embedding.

Closely related embeddings, differing only in the additive global torsion, can be obtained by $\mathbf{n}(t) \rightarrow \mathbf{n}'(t)$, $\mathbf{b}(t) \rightarrow \mathbf{b}'(t)$, where $\mathbf{n}'(t)$ and $\mathbf{b}'(t)$, are obtained from the normal and binormal by rotation :

$$\begin{bmatrix} \mathbf{n}'(t) \\ \mathbf{b}'(t) \end{bmatrix} = \begin{bmatrix} \cos(mt) & \sin(mt) \\ -\sin(mt) & \cos(mt) \end{bmatrix} \begin{bmatrix} \mathbf{n}(t) \\ \mathbf{b}(t) \end{bmatrix}$$

The global torsion changes by m, when m is an integer. Noninteger rational values of m provide a mapping from $D^2 \times S^1 \rightarrow R^3$ that is not an embedding, and whose properties remain to be studied. In the simplest case that the carrier knot is a simple planar circle, the embedding with $m = 0$ is the preferred embedding and those with $m \neq 0$ differ from the preferred embedding by global torsion m [27].

5 Embeddings of Data

Embeddings are the primary tools used to analyze experimental data. Data from low-dimensional dynamical systems usually comes in the form of a scalar time series. This series must be embedded in a higher-dimensional space in order to study a strange attractor (if there is one). A number of embedding theorems exist. They all owe their origins to the original embedding theorem of Whitney. He proved that *every* n-dimensional manifold can be embedded in R^N with $N \geq 2n+1$ [28]. He later reduced this bound to $N \geq 2n$ [29].

Embedding theorems were introduced into dynamical systems theory by Packard *et al.* and by Takens [30], [31]. These authors showed that the geometry of a chaotic attractor could always be recovered from scalar time series by embedding the time series in R^N using $N-1$ time delays, provided $N \geq 2n+1$.

Embedding theorems concentrate on the wrong questions [27]. A better set of questions is :

Dimensions : Determine a k-parameter family of mappings of the scalar time series into R^m (or some m-dimensional manifold), where $m \leq n$ is the dimension of the *inertial manifold* that contains the strange attractor [19]. The k parameters could be (unequal) time delays, or other. Identify open domains (embedding islands) in the k-dimensional parameter space that provide embeddings.

Topology : Determine the topology of the embedded attractor in the embedding islands. How does this topology vary from island to island ?

One question that has been asked since the first days of Topological Analyses has been : "What is the relation between the topology of the embedded attractor and the attractor (unseen) that generated the chaotic time series in the first place ?" It appears that we are nearing a useful answer to this question for low-dimensional attractors. We outline the arguments for this claim.

We assume the "experimental attractor" has dimension $d_L < 3$, and that we have found an embedding island for an embedding into R^3. We assume that this island is stable : We have an embedding for all experimental values from the "laminar" to the "fully chaotic" regime (see above).

The spectrum of unstable periodic orbits in any chaotic data set is independent of the embedding [4], [5]. As a result, there is a 1-1 correspondence between the unstable periodic orbits in the original attractor and in its embedding. Orbit forcing in the two attractors is identical. Since orbit forcing is unique to the perestroikas of a branched manifold (this hope remains to be proved), the two branched manifolds must reflect the same stretching and squeezing mechanisms. Thus, they can only differ by :

Parity : Handedness (mirror images exhibit equivalent, non isotopic orbit organization).

Global Torsion : For a branched manifold contained in a genus-one bounding torus, or the analog for higher genus.

Knot type : Different extrinsic embeddings (into R^3) of the same intrinsic structure follow different, nonisotopic, Fourier knots.

If the dynamics is generated by a horseshoe mechanism, any embedding of the data will produce an embedded strange attractor that projects to a branched manifold that exhibits a horseshoe. The only degrees of freedom in this embedded horseshoe are : handedness, global torsion, and knot type. This theorem is summarized by the colorful statement : "Once a horseshoe, always a horseshoe."

6 All the Covers of the Horseshoe

In the theory of Lie groups there is a beautiful theorem due to Elie Cartan. It relates universal covering groups with their locally isomorphic image Lie groups. Specifically, this theory states that of all the Lie groups (think : $SU(2)$ and $SO(3)$, for example) with "the same" Lie algebra, there is a 1-1 correspondence between the Lie algebra and only one of these groups (think $SU(2)$), the one that is simply connected. All the others are *images* of the universal covering group by one of its discrete invariant subgroups ($SO(3) = SU(2)/\{I_2, -I_2\}$). The cover and image groups are related by $p \to 1$ local isomorphisms.

It has been pointed out that the questions asked in the development of both Lie group theory and singularity theory are very similar, and similar to the questions that ought to be asked of the nascent field of dynamical systems [5]. A natural question is : "What is the analog of Cartan's theorem for dynamical systems ?"

Letellier and his colleagues have studied groups and dynamical systems extensively. They have been particularly interested in equivariant dynamical systems (systems with symmetry), and in particular the cover-image relation. It is clear that the "locally isomorphic" of Lie group theory translates into "locally diffeomorphic" in dynamical systems theory, and that $p \to 1$ image, $p \leftarrow 1$ lift (or cover), are the same in both fields. A number of covers of the Rössler system have been exhibited [22]. Some are structurally unstable, others are structurally stable.

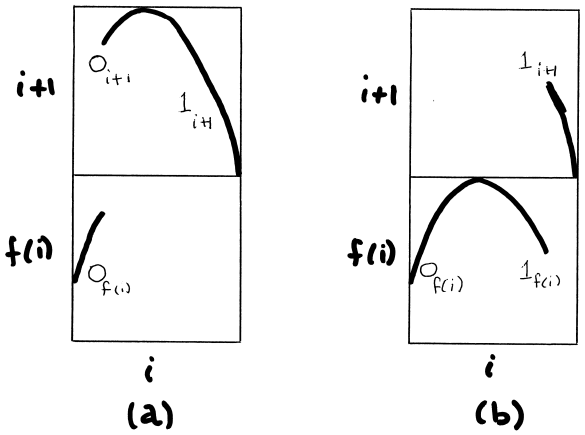

Fig.9. Return maps for covers of the horseshoe. Bare return maps over all branch lines are identical : they can differ only by their dressing labels. Torsion information determines layering information, so only torsion is necessary to dress the full return map of any cover. All these covers are structurally unstable against the location of the splitting point.

We now are able to answer the question of this Section. We begin with a horseshoe branched manifold, for example, generated by the Rössler attractor, in the bounding torus A_1. We look for lifts of this into an arbitrary bounding torus of genus g. The $g-1$ branch lines in the cover branched manifold will all be identified with the single branch line of the image. The cover-image relation is effected by a $(g-1) \to 1$ local diffeomorphism. Every lift has a return map of the form shown in Fig. 9. This figure shows that part of the outflow from branch i flows to branch $i+1$ under $T_{\rm cyc}$, and part flows to branch $f(i)$ under $T_{\rm str}$.

The zero-torsion part (positive slope) of the original branched manifold lifts to the zero torsion part in the cover. The torsion-1 part of the branched manifold lifts to the negative sloped part in the cover. This can have torsion either $+1$ or -1. Each of the panels over the $g-1$ branch lines must be "dressed" with an integer, ± 1, identifying the torsion of the orientation-reversing branch leaving branch line i. The way in which the zero-torsion and ± 1-torsion incoming branches are joined at branch line j is determined by the torsion of the incoming branch. Thus, this piece of information is already contained in the "torsion dressing information" attached to the negative sloped branches over branch line i.

Given a canonical bounding torus of genus g, there are 2^{g-1} lifts of the horseshoe into this bounding torus. They are not all necessarily inequivalent. If the bounding torus has symmetry some of the lifts are equivalent. For example, the genus-4 bounding torus C_3 has three-fold rotation symmetry under the group C_3, so the $8 = 2^3$ lifts break up into $4 = 3 + 1$ different equivalence classes of inequivalent lifts. Two classes are mirror images of the other two.

All the lifts with return maps as given in Fig. 9 are structurally unstable under perturbatin of the singularity that tears the flow. Structurally stable lifts are obtained by closing off all the "internal" flow tubes (identified by $T_{\rm str}$) or all the "external" flow tubes (identified by $T_{\rm cyc}$). The return maps in these two cases are shown in Fig. 10(a) and (b). We illustrate what happens in the case of structurally stable lifts of the horseshoe into the genus-6 branched manifold 11212 with $(g, m) = (6, 4)$ shown in Fig. 7.

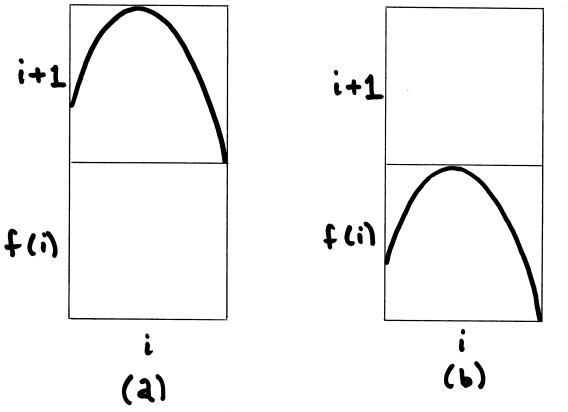

Fig.10. Structurally stable return maps for covers of the horseshoe. (a) Interior flow tubes are blocked off (cf. Fig. 11). (b) Exterior flow tubes are blocked off (cf. Fig. 12).

When all the internal flow tubes are closed off (Fig. 11), the flow occurs in a genus-one bounding torus. The five original branch lines can be moved together : the resulting branched manifold now has 2^{6-1} branches instead of the original $2 \times (6-1)$. There are eight equivalence classes of inequivalent lifts, which occur as four mirror image pairs.

When the external flow tubes are closed off (Fig. 12), the flow is "fully reducible." It is restricted to $m = 4$ disconnected bounding tori of type A_1. Three inherit one branch line each, and one inherits two. The description of these covers mirrors exactly the description of fully reducible representations of groups.

We conclude that the analog of Cartan's theorem for dynamical systems is the inverse of his theorem for Lie groups. There is one universal *image* dynamical system with a countable number of locally diffeomorphic but inequivalent covers. For any genus g, there are $N(g)$ canonical bounding tori. For any one of them, there are 2^{g-1} lifts with return maps of the type shown in Fig. 9. They are all structurally unstable. In the structurally stable case there are two possibilities : (a) The flow remains irreducible in a torus of type A_1 with $g-1$ branch lines that can be consolidated into one; (b) The flow is fully reducible

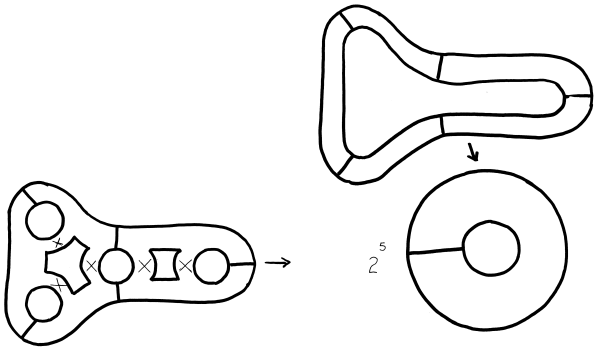

Fig.11. Flow through all interior flow tubes is restricted. This is shown by the $\times$. The residual flow is through a bounding torus of type A_1 with 5 branch lines and 10 branches. They can be consolidated into a single branch line serving 32 branches.

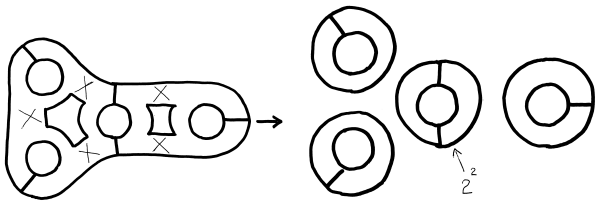

Fig.12. Flow through all exterior flow tubes is restricted. This is shown by the $\times$. The residual flow is disconnected (fully reducible), contained in four ($= m$) bounding tori of type A_1. Of these, three have a single branch line and two branches and one has 2 branches with 2×2 branch lines. The two branch lines can be consolidated, giving a flow with one branch line and 2^2 branches.

into disconnected flows in m bounding tori, each of type A_1. The number of branch lines attached to the branched manifold within each of the A_1 is determined by inspection of the original bounding torus.

7 Summary & Conclusions

At the present time a great deal is known about a limited class of strange attractors. This is the class of low-dimensional strange attractors : those with Lyapunov dimension $d_L < 3$, which exist in three dimensional manifolds, for example R^3. This knowledge was obtained by exploiting the insights made by Poincaré more than one hundred years ago, as well as studying large numbers of attractors belonging to this class. These include the Lorenz attractor and the Rössler attractor, as well as two previously studied forced damped oscillators that generate complicated time series : the Duffing and the van der Pol oscillators. Poincaré's insights emphasized the use of topological tools for the study of these systems, and pointed out that unstable periodic orbits were the most promising tool available for understanding the global topological structure of strange attractors.

We have exploited these insights to develop what appears to be a complete hierarchy of structures that are useful for classifying strange attractors in three dimensions. The four levels of structure are :

1. Basis sets of orbits, that force all the periodic orbits present in a strange attractor.
2. Branched manifolds, that organize all the periodic orbits present in a strange attractor.
3. Bounding tori, that organize branched manifolds in the same way that branched manifolds organize unstable periodic orbits.

4. Extrinsic embeddings, that describe how bounding tori are embedded in the ambient three dimensional manifold (e.g., R^3).

We do not yet have a complete understanding of all these areas. Basis sets of orbits are known, to low period, for the Smale horseshoe mechanism. They are not known for other mechanisms. Branched manifolds are much better understood. However, there is a theory of "representations of branched manifolds," in analogy with the theory of the representations of groups, that does not yet exist. This seeks to classify all the branched manifolds that give rise to isomorphic spectra of orbits and orbit organization. Through truly fortuitous circumstances, we have a complete understanding of (intrinsic) bounding tori. We have a limited understanding of extrinsic embeddings of bounding tori into R^3. In the genus-one case we have made remarkable progress. We hope to extend this understanding to the higher genus case in the near future.

Classification of strange attractors in R^3 is possible due to a number of "lucky accidents." The first is that knots (=periodic orbits) link nontrivially in three-dimensional spaces. This allows us to exploit their topological organization to identify the branched manifold that holds them. This also allows us to construct forcing relations, and to introduce the idea of a basis set of orbits.

It is possible to completely classify bounding tori because of two 'lucky' breaks. The first is that in three dimensional dissipative dynamical systems that generate chaos, there is always one positive Lyapunov exponent and one negative Lyapunov exponent. The second lucky break is that surfaces that enclose strange attractors (closed, boundaryless, orientable) have all been classified, and are boundaries of genus-g handlebodies (tori with g holes). The flow, restricted to these surfaces, has fixed points with one stable and one unstable direction. They are all saddles. This gives a rigidity to the number of singularities — through the Euler characteristic and the Poincaré-Hopf index theorem — that we cannot expect to find in higher dimensions. In particular, the beautiful result that there are $g-1$ pairs of "splitting"-"joining" singularities distributed over the genus-g surface will not exist for higher dimensions. Finally, we have a head start in our understanding of how these handlebodies can be embedded in R^3 through knots. That is, a genus-one bounding torus can be embedded in R^3 by mapping its centerline along any knot with reasonable properties. So in this case the embedding question is related to the problem of enumerating knots in R^3. There are other degrees of freedom in such embeddings, such as self linking numbers and global torsion that still need to be better understood. The extension to embeddings of genus-g tori should be only slightly more complicated.

We hope to use this spectrum of results for strange attractors in R^3 as a model for understanding how to go about classifying strange attractors in higher dimensions. There are many obstructions to this program. The first and greatest is that knots "fall apart" in R^n, $n > 3$. There is the hope to create a "knotless linking theory" that is currently in progress [32]. We hope a speedy, successful implementation will occur. Another major problem is that in R^4 it is possible to have strange attractors with two positive and one negative (local) Lyapunov exponents, or *vice versa*, or even both cases in a single attractor. This is a problem because saddles distributed over three-dimensional over bounding surfaces of four-dimensional attractors could have both positive and negative indices, so our rigid result (Euler-Poincaré) for two-dimensional bounding tori is not easily extendable.

But the most problematic result is that there is no classification result for three-dimensional closed, boundaryless, orientable surfaces in R^4 as there is for the two-dimensional case in R^3. This is closely related to the Poincaré conjecture.

In concluding, we get right back to where we began : with Poincaré. His conjectures initiated this field in its modern guise. To continue into higher dimensions we must resolve and extend his most famous unsolved conjecture.

Acknowledgements : It is a pleasure to thank S. Bielawski, G. Byrne, M. Lefranc, C. Letellier, G. B. Mindlin, A. Nishtala, H. G. Solari, and T. D. Tsankov for exciting interactions and useful comments. The author thanks C. Letellier for helping to organize this Colloq. This work was partially supported by NSF Grant PHY-9987468.

Références

1. H. Poincaré, *Les méthodes nouvelles de la mécanique céleste*, Gauthier-Vilars, Paris, 1899.
2. E. N. Lorenz, Deterministic nonperiodic flow, *J. Atmos. Sci.*, **20** , 130-141 (1963).
3. O. E. Rössler, An equation for continuous chaos, *Phys. Lett. A***57** , 397-398, (1976).
4. R. Gilmore, Topological analysis of chaotic dynamical systems, *Revs. Mod. Phys.* **70**(4), 1455-1529 (1998).
5. R. Gilmore and M. Lefranc, *The Topology of Chaos*, Wiley, New York, 2002.
6. V. I. Arnol'd, A. Varchenko, and A. Gousein-Zadé, *Singularitiés des applications differentiales*, Editions Mir, Moscou, 1986.
7. C. Wei *The Cusp Singularity in Nonlinear Dynamical Systems*, Thesis, Drexel University, 2003.
8. J. Birman and R. F. Williams, Knotted periodic orbits in dynamical systems II : Knot holders for fibered knots, *Cont. Math.* **20**, 1-60 (1983).
9. H. G. Solari and R. Gilmore, Relative rotation rates in driven dynamical systems, *Phys. Rev.* **A37**, 3096-3109 (1988).
10. G. B. Mindlin, X.-J. Hou, H. G. Solari, R. Gilmore, and N. B. Tufillaro, Classification of strange attractors by integers, *Phys. Rev. Lett.* **64**, 2350-2353 (1990).
11. N. B. Tufillaro, H. G. Solari, and R. Gilmore, Relative rotation rates : Fingerprints for strange attractors, *Phys. Rev.* **A41**, 5717-5720 (1990).
12. G. B. Mindlin, H. G. Solari, M. A. Natiello, R. Gilmore, and X.-J. Hou, Topological analysis of chaotic time series data from the Belousov-Zhabotinskii reaction, *J. Nonlin. Sci.* **1**, 147-173 (1991).
13. F. Papoff, A. Fioretti, E. Arimondo, G. B. Mindlin, H. G. Solari, and R. Gilmore, Structure of chaos in the laser with saturable absorber *Phys. Rev. Lett.* **68**, 1128-1131 (1992).
14. G. B. Mindlin, R. Lopez-Ruiz, H. G. Solari, and R. Gilmore, Horseshoe implications, *Phys. Rev.* **E48**(6), 4297-4304 (1993).
15. T. Hall, Weak universality in two-dimensional transitions to chaos, *Phys. Rev. Lett.* **71**(1), 58-61 (1993).
16. T. Hall, The creation of horseshoes, *Nonlinearity* **7**, 861-924 (1993).
17. T. D. Tsankov and R. Gilmore, Strange attractors are classified by bounding tori, *Phys. Rev. Lett.* **91**(13), 134104 (2003).
18. T. D. Tsankov and R. Gilmore, Topological aspects of the structure of chaotic attractors in R^3, *Physical Review* **E** (to be submitted).
19. J.-P. Eckmann and D. Ruelle, Ergodic theory of chaos and strange attractors, *Revs. Mod. Phys.* **57**(3), 617-656 (1985).
20. Jeffrey R. Weeks, *The Shape of Space* (Second Edition), Marcel Dekker, New York, 2002.
21. V. I. Arnol'd *Ordinary Differential Equations*, MIT Press, Cambridge, MA, 1989.
22. R. Gilmore and C. Letellier, *The Symmetry of Chaos*, (to be published).
23. D. Rolfsen, *Knots and Links*, Publish or Perish, Berkeley, 1976.
24. M. A. Aziz-Alaoui, Differential equations with multispiral attractors, *Int. J. Bifurcation and Chaos* **9**(6), 1009-1039 (1999).
25. R. Miranda & E. Stone, The proto-Lorenz system, *Physics Letters* **A178**, 105-113, 1993.
26. C. Letellier & R. Gilmore, Dressed symbolic dynamics, *Physical Review* **E67**, 036205 (2003).
27. T. D. Tsankov, A. Nishtala, and R. Gilmore, Embeddings of a strange attractor into R^3, *Physical Review* **E** (submitted).
28. H. Whitney, Differentiable manifolds, *Ann. Math.* **37**, 645 (1936).
29. H. Whitney, The self-intersections of a smooth n-dimensional manifold in $2n$ space, *Ann. Math.* **45**, 247 (1944).
30. N. Packard, J. Crutchfield, D. Farmer, and R. Shaw, Geometry from time series, *Phys. Rev. Lett.* **45**, 712-715 (1980).
31. F. Takens, Detecting Strange Attractors in Turbulence, *Lecture Notes in Mathematics, Vol.* **898**, Springer-Verlag, Berlin, 1981 : pp. 366-381.
32. M. Lefranc, private communication.